4, 880 (1962)]. Our e_{ij}'s are the strain elements and should not be confused with the ϵ's in this reference which are related to our G's; i.e., Tucker (Ref. 42) gives the correspondence $G_{11}=\frac{4}{3}\epsilon_2 R$, $G_{44}=\epsilon_5 R$.

[44]R. D. Mattuck and M. W. P. Strandberg, Phys. Rev. 119, 1204 (1960).

PHYSICAL REVIEW B VOLUME 6, NUMBER 5 1 SEPTEMBER 1972

Neutron-Scattering Study of the Ferroelectric Phase Transformation in $Tb_2(MoO_4)_3$ †

B. Dorner,* J. D. Axe, and G. Shirane
Brookhaven National Laboratory, Upton, New York 11973
(Received 24 April 1972)

We establish a first example of a ferroelectric phase transformation where a Brillouin-zone-boundary soft mode [at the M point $(\frac{1}{2},\frac{1}{2},0)$] rather than a Brillouin-zone-center mode of the parent paraelectric phase (PE) is responsible for the transition. By inelastic scattering of neutrons, we have measured low-frequency phonon-dispersion relations in $Tb_2(MoO_4)_3$ for symmetry directions emanating from the M point in PE. For $T > T_0 = 159\,°C$ the frequency ω_M of a doubly degenerate mode at M follows a Curie-Weiss law $\omega_M^2 = A(T - T_C)$, with $A = 0.0165$ meV^2/°C and $T_C = 149\,°C$. With the help of group theory, the symmetry properties of soft modes which lead from the PE symmetry (tetragonal $P\bar{4}2_1m$) to the symmetry (orthorhombic $Pba2$) of the ferroelectric (FE) phase were determined. The soft-mode eigenvectors contain parameters which are not fixed by symmetry and their "static" values can be obtained from existing x-ray–structure data. "Dynamic" values are determined here from the integrated inelastic-scattering intensity of the soft mode measured in PE at various M points. The "static" and the "dynamic" values are in good agreement. The condensation of such an antiferroelectric soft mode cannot directly produce the spontaneous polarization P_z in FE. As has been suggested theoretically, our measurements show that the antiferroelectric static displacements constitute the order parameter, which couples to a shear strain u_{xy}, which in turn produces the polarization by piezoelectric coupling. The spontaneous polarization and the spontaneous strain in FE are shown to be proportional to the square of this order parameter. From the initial slopes of acoustic branches we derive a set of elastic constants in PE.

I. INTRODUCTION

Several rare-earth molybdates were discovered by Borchardt and Bierstedt[1] to undergo ferroelectric phase transformations at transition temperatures $150 < T < 190\,°C$. These materials[2,3] show many unusual properties. In a stress-free crystal, a small dielectric anomaly is found at low frequencies in the ferroelectric phase (FE). In the high-temperature paraelectric phase (PE) the dielectric constant is independent of temperature. On the other hand, the clamped crystal does not show a dielectric anomaly at all.[4] Similarly, the elastic properties show an anomaly below the transition only.[4,5] Coupled with spontaneous polarization states of opposite polarity ($\pm P_z$, which of course can be switched by an applied electric field)[6] are two mechanical configurations described by a shear strain $\pm u_{xy}$ (see Fig. 1). One mechanical configuration can be switched into another by an applied mechanical stress.[7] This has been described as ferroelastic behavior.[8] But ferroelectricity and ferroelasticity in this material are so coupled that P_z and u_{xy} change simultaneously.

The coupling of elastic and dielectric properties, together with the absence of a dielectric anomaly in the clamped crystal, led Cross *et al.*[4] to the conclusion that the spontaneous polarization was an incidental but necessary consequence of the strain u_{xy}, since the piezoelectric constant a_{36} (coordinates of PE) is nonzero.[5,9] Pytte,[10] however, suggested that this picture was incomplete and that the transition is fundamentally connected with a doubly degenerate soft mode at the Brillouin-zone edge in PE, which leads to a doubling of the unit cell. Independently, Levanyuk and Sannikov[11] and Aizu[12] came to the same conclusion.

The only experimental technique capable of direct investigation of such a proposed mechanism is that of inelastic neutron scattering. This paper presents such a study. A preliminary account of this work has already been reported.[13] When this work was begun, some uncertainty existed in the literature concerning the sizes of the PE and FE unit cells. In preliminary experiments, we therefore established that the anticipated doubling of the cell volume does in fact occur. Subsequently reliable structure determinations in the FE phase of isostructural $Gd_2(MoO_4)_3$ (GMO) by Keve *et al.*[14] and in both phases by Jeitschko[15] have been reported. The recent data are in substantial agreement with those given in Table I for $Tb_2(MoO_4)_3$ (TMO).[16–18]

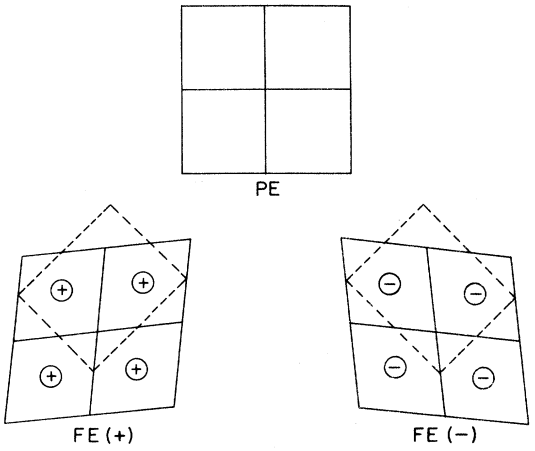

FIG. 1. Schematic drawing of the two possible configurations in FE coming from PE. The solid lines describe unit cells of PE and the dashed lines those of FE projected onto the x-y plane. The (+) and (−) indicate the direction of the spontaneous polarization along z.

In Sec. II we report measured phonon-dispersion relations, which indicate a soft mode at the M point $(\frac{1}{2}, \frac{1}{2}, 0)$. The temperature dependence of this soft mode was measured over a wide range ($T_0 < T < 725\,^\circ$C) and establishes a phonon instability at the M point. In Sec. III we use a group-theoretical approach[19] to derive a system of basis vectors $\vec{e}_i$ used in construction of atomic displacements in PE, which lead to the FE symmetry. The eigenvectors $\vec{E}_i$ of the doubly degenerate soft mode in PE are linear combinations of the $\vec{e}_i$. An inelastic-structure analysis was performed to determine the proper linear combinations of the $\vec{e}_i$ in the $\vec{E}_i$.

A Brillouin-zone-boundary mode is generally "antiferroelectric" and cannot directly produce a spontaneous polarization. In Sec. IV we report the measured temperature dependence of the antiferroelectric static displacements, which are the order parameters in TMO. A somewhat simplified free-energy expansion is considered in order to understand the origin of the polarization and its relation to the primary order parameter. Finally, in Sec. V we compare a set of "high-frequency" elastic constants derived from our measurements with ultrasonic results.[20]

TABLE I. Crystallographic data for $Tb_2(MoO_4)_3$ above and below the transition temperature $T_0 = 159\,^\circ$C, Refs. 16–18.

Space group	Lattice constant (Å)			Formula units per unit cell
	a	b	c	
$T > T_0$ Tetragonal $P\bar{4}2_1m$	7.37	7.37	10.62	2
$T < T_0$ Orthorhombic $Pba2$	10.35	10.38	10.66	4

Our studies were carried out at the Brookhaven National Laboratory high-flux-beam reactor with a single crystal of $0.8 \times 1.0 \times 2.5$ cm for the inelastic measurements, loaned to us by Brixner.

II. WAVE-VECTOR AND TEMPERATURE DEPENDENCE OF SOFT MODE

A study of the structural information given in Fig. 2 and Table I reveals that the reduction in the translational symmetry necessary to pass from PE to FE must result from displacements modulated with the wave vector $\vec{q}_M = (\frac{1}{2}, \frac{1}{2}, 0)$ in PE. We have therefore determined the dispersion of several phonon branches in the PE phase lying along symmetry lines in the (hk0) plane and connecting with the condensing wave vector $\vec{q}_M$. On a structure as complex as TMO, it is clearly impractical to carry out an exhaustive mapping out of phonon branches by inelastic neutron scattering. However, in order to establish the occurrence of instabilities leading to a displacive phase transformation it is sufficient to measure the low-lying branches. The results are shown in Fig. 3. The phonon instability appears clearly at the M point. We find inelastic scattering from this soft mode at every $\vec{Q} = \vec{G}_{PE} + \vec{q}_M$, where $\vec{G}_{PE}$ is a reciprocal-lattice vector of PE. This intensity is particularly large at $\vec{Q} = (\frac{5}{2}, \frac{9}{2}, 0)$.

At temperatures near to the transition, the soft

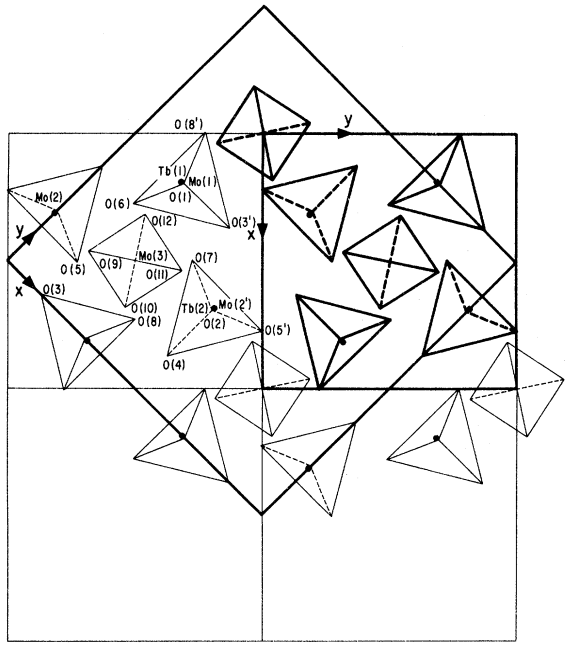

FIG. 2. Tetragonal (PE) and orthohombic (FE) unit cell projected onto x-y plane. The molecular orientation is as in PE. The dots • give the Tb positions and the tetrahedra represent MoO_4 groups. Atom designation is taken from Jeitschko (Ref. 15). For atomic displacements see Table III.

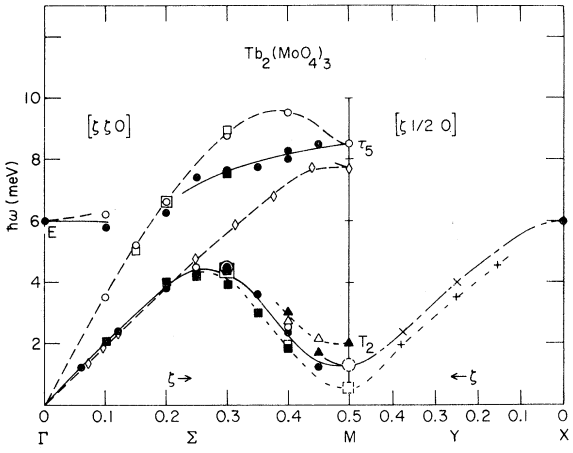

FIG. 3. Measured phonon dispersion. Phonons labeled Σ_1(---) and Σ_2(——) are, respectively, even and odd under reflection in the $(\zeta\bar{\zeta}0)$ plane. Open symbols indicate measurements with $\vec{Q} \parallel \vec{q}$ ("longitudinal"), closed symbols $\vec{Q} \perp \vec{q}$ ("transverse") in an (hk0) plane. ◇ indicates $\vec{Q} \perp \vec{q}$, but in another orientation of the sample (*hhl*). There was no simple relation between Q and q for the remaining points. ○, ●, and × are measured at 260 °C; □, ◇, and + at 184 °C; and △ at 400 °C.

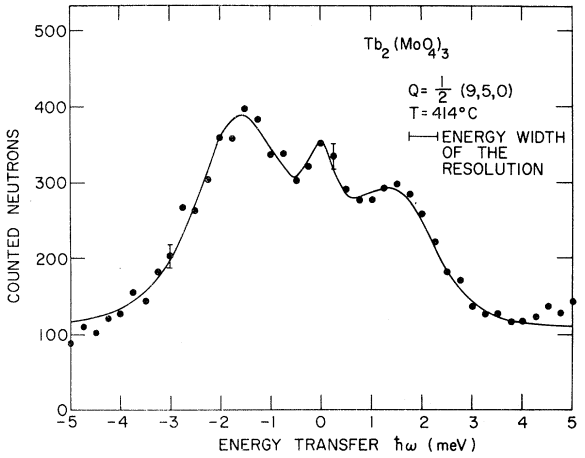

FIG. 4. Energy profile of the inelastic "critical" scattering at a superlattice point in PE. The central peak is due to higher-order contamination of the incident beam. The solid curve represents a least-squares fit of Eqs. (1) and (2). The asymmetry is entirely due to resolution effects.

mode is overdamped. It is possible to separate distinct maxima for energy gain and loss processes only at temperatures more than 200 °C above the transition.[13] Figure 4 shows results at 414 °C. The data can be interpreted by a scattering law $S(\vec{Q}, \omega)$ for a damped harmonic oscillator, which has the form

$$S(\vec{Q}, \omega) \propto \frac{k_B T \Gamma}{(\omega_M^2 - \omega^2)^2 + \omega^2 \Gamma^2} \left| F_{\text{inel}}(\vec{Q}) \right|^2 . \tag{1}$$

Here ω_M is the quasiharmonic frequency and Γ is a damping parameter. This scattering law, written for energy transfers $\hbar\omega \ll k_B T$, is fulfilled in this case. To perform a least-squares fit to the measured intensities $I(Q_0, \omega_0)$ we used the expression

$$I(\vec{Q}_0, \omega_0) = \int R(\vec{Q} - \vec{Q}_0, \omega - \omega_0) S(\vec{Q}, \omega) d^3Q \, d\omega , \tag{2}$$

where R is the resolution function[21] containing the experimentally determined reflectivity[22] of the analyzing pyrolytic-graphite crystal. The very good fit was obtained by using an accurate normalization[23] of R. The asymmetry is produced entirely by resolution. The peak at $\omega = 0$ arises from higher-order contamination in the beam (this point was checked by inserting additional filtering[24]) and was described in the fit by an additional Gaussian function.

We performed similar measurements at several temperatures up to 725 °C, which is close to the α-β phase transition.[3] As shown in Fig. 5, over this region $\omega_M(T)$ is consistent with the Curie-law behavior

$$(\hbar\omega_M)^2 = A(T - T_C) , \tag{3}$$

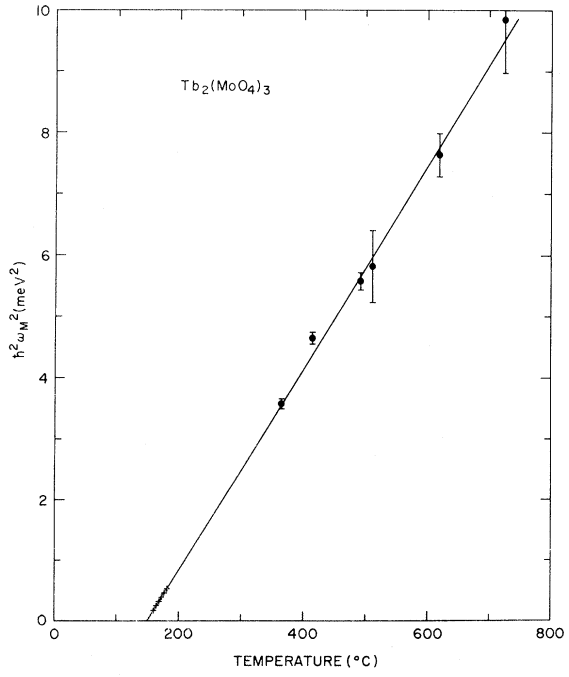

FIG. 5. Temperature dependence of the frequency of the soft mode ω_M at the M point. At higher temperatures, ω_M was determined by fitting the spectral profiles (Fig. 4) to Eq. (1). The lower-temperature data (×'s) were obtained from the temperature dependence of the integrated intensity, as explained in Ref. 13.

which approximately characterizes all known soft-mode behavior[25] with $A = (1.65 \pm 0.10) \times 10^{-2}$ meV^2/°C and $T_C = (149 \pm 2)$ °C. Γ was found to be about (2.5 ± 0.5) meV, and within the statistical errors independent of temperature. The value of A reported in the preliminary work[13] was somewhat larger due to the presence of a small misoriented crystal which was masked off in the later work.

In constructing the smoothed dispersion relations through the observed points in Fig. 3, we have included a "longitudinal" and "transverse" notation which has a practical experimental relevance, although in a complicated system like TMO it can be justified only in the $q \to 0$ limit for acoustic branches. Since not all branches are complete, it is possible that the curves drawn are in reality only quasi-continuous in the sense that other branches of like symmetry may "cross" them with a resultant small splitting. Where symmetry considerations dictate a splitting of bands degenerate at the Γ or M points, this fact is noted by a short line, if both branches were not actually seen.

It is not possible to fit together existing optical and neutron data in a completely unambiguous way, but symmetry arguments are helpful in putting together a partial picture. Compatibility relations connecting the various symmetry points of interest are shown in Fig. 6. We may probably associate the 6-meV phonon which we observe at $q = 0$ in PE with the B_1 mode in FE seen by infrared[26,27] and Raman[28] scattering at 6.2 meV, which does not shift with temperature[28] and persists into PE,[26] where it becomes an E mode. Another infrared-active mode at $q = 0$ in FE disappears in PE and thus presumably becomes a τ_5 mode at the M point.[26,27] This could be the M-point mode we observe at either 7.7 or 8.5 meV. The latter mode has τ_5 symmetry; the former is either T_1 or τ_5.

We have also extended our measurements of the soft mode into the FE phase. Here we expect the soft-mode scattering to be largest around (and have intensity proportional to) the superlattice reflections. We therefore chose the strong (7, 2, 0) superlattice reflection [$(\frac{5}{2}, \frac{9}{2}, 0)$ in PE] and performed E scans at five different temperatures over an energy transfer of $+2.0 \geq \hbar\omega \geq -9.0$ meV. For small energy transfer ($\geq |0.25$ meV$|$) the intensity decreases with increasing temperature in agreement with the temperature dependence of the elastic superlattice intensity as discussed in Sec. IV. But for larger nominal energy transfer the intensity first slightly decreases with increasing temperature but then increases when approaching the transition temperature. We associate this latter component with inelastic critical scattering from the soft phonons. In order to approximately separate elastic and inelastic components we assume that at room temperature $I_{\text{Bragg}} \gg I_{\text{inel}}$ for all $|\hbar\omega|$ up to 3 meV. This approximation means that the energy profile around $\hbar\omega = 0$ at room temperature represents only Bragg scattering convoluted with the resolution. Since we know accurately the temperature dependence of this elastic scattering, it is then a simple matter to subtract this elastic contribution from higher-temperature measurements. (If anything, this slightly overestimates the elastic contribution.) It is felt that this correction was reliable for data with $\hbar\omega > 0.75$ meV.

After subtraction of the elastic scattering there remains a central cross section as well as a reasonably well-defined phonon peak at 5.7 meV. We assume a scattering law for the well-resolved peak of the form of Eq. (1) with parameters F_1, ω_1, Γ_1, allowing the latter two to vary with temperature. Simultaneously, we tried to fit the residual low-frequency scattering with F_2, ω_2, Γ_2. The fitted data (including resolution effects) are shown in Fig. 7. The parameters of the low-frequency peak were not uniquely determined and we can only conclude that $\omega_2 \ll \Gamma_2 \sim 2$ meV. A reliable fit was, however, obtained for the higher-energy peak. The ω_1 and Γ_1 are shown in Fig. 8.

At room temperature the value $\hbar\omega_1 = 5.7$ meV, which we determine is very close to that of the A_1-mode found by Fleury[28] at 5.9 meV, with our results showing a somewhat stronger temperature

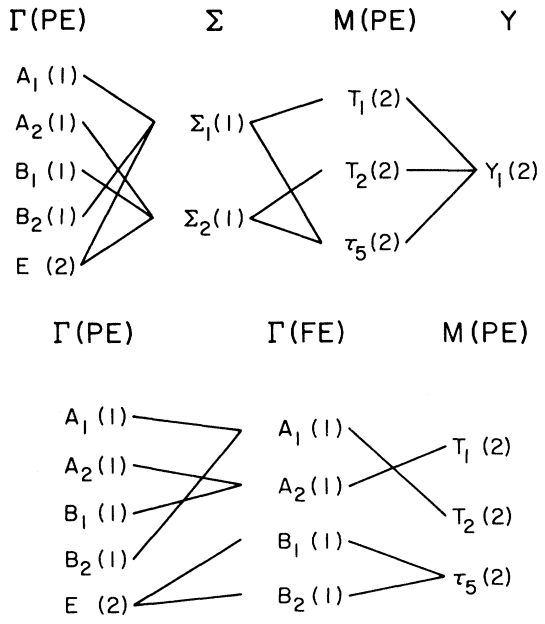

FIG. 6. Compatibility relations between Γ point (0, 0, 0), Σ direction $[\zeta, \zeta, 0]$, M point $(\frac{1}{2}, \frac{1}{2}, 0)$, and y direction $[\zeta, \frac{1}{2}, 0]$. The representations T_1, T_2, and τ_5 are given in Table II. The degeneracy is indicated in parentheses. Note that the group of Y has but a single doubly degenerate representation Y_1. Compatibility relations from Γ(PE) and M(PE) to Γ(FE) are given below.

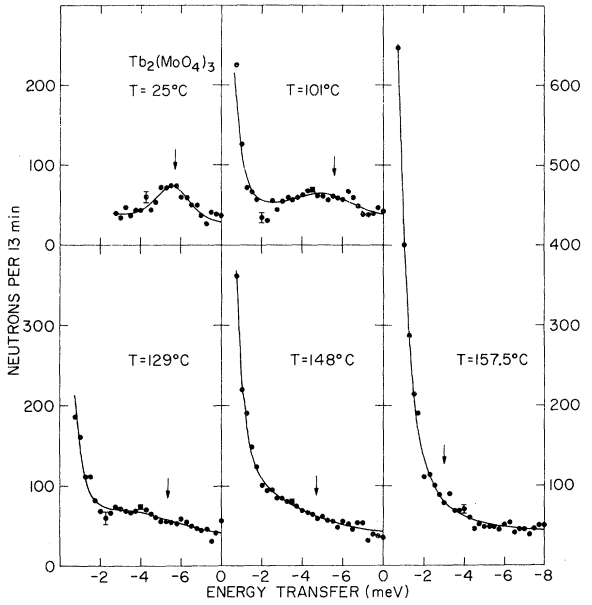

FIG. 7. Energy scans (energy gain of the neutrons) at $\vec{Q} = (7, 2, 0)$ (FE indexing) for several temperatures. The errors are smaller for $\Delta E \geq 3$ meV due to better statistics. Contributions from Bragg scattering are subtracted in the region $\Delta E \leq 3$ meV. The solid curves represent a least-squares fit of two excitations with frequencies ω_1 (indicated by arrows) and ω_2 (< 1 meV) by means of Eqs. (1) and (2).

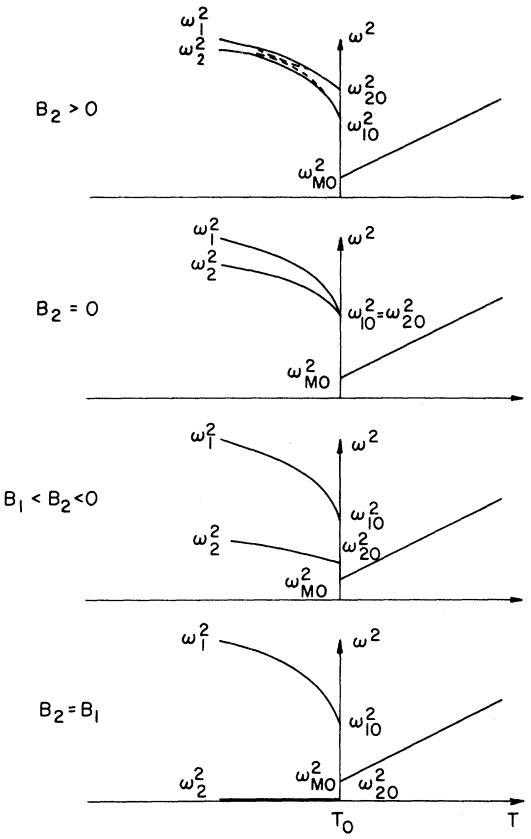

FIG. 9. Soft-mode frequencies in PE and FE. Doubly degenerate modes show Curie-Weiss behavior above T_0. Below T_0, the degeneracy is removed between mode 1 (eigenvector proportional to static displacements) and the orthogonal mode 2. ω_{10} and ω_{20} are the limiting values of ω_1 and ω_2 as T_0 is approached from below. The precise behavior of the modes below T_0 depends upon the detailed form of the free energy (see Appendix).

dependence. Infrared measurements by Petzelt[27] with polarized light also reveal a broad A_1 excitation near 5.7 meV at room temperature, which was resolved into two A_1 modes at lower temperatures. He observed that the frequencies of these modes decrease slightly with increasing temperature and

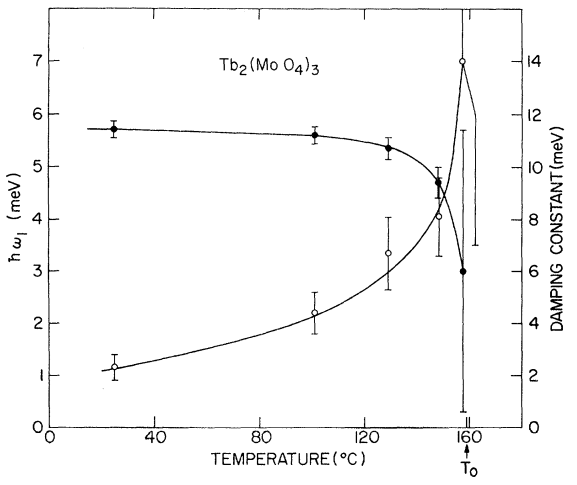

FIG. 8. Temperature dependence of the energy $\hbar\omega_1$ (closed circles) and damping constant Γ_1 (open circles) derived from the data of Fig. 7.

the oscillator strength vanishes as $(T_0 - T)$.

Very generally, the soft mode in FE must be totally symmetric (A_1).[29] From Fig. 6 the doubly degenerate soft modes in PE become two nondegenerate A_1 modes in FE. The two frequencies ω_1 and ω_2 depend on the higher-order terms in the free energy of the system and on temperature. This behavior is discussed more explicitly in the Appendix and some examples of possible behavior are shown in Fig. 9. One of these two A_1 modes with frequency ω_1 has an eigenvector similar to the vector of the condensed static displacements, which in turn is similar to one of the eigenvectors of the doubly degenerate soft modes in PE.

It does not seem possible to deduce unambiguously the behavior of the soft modes in FE as yet. Petzelt[27] considered the two modes which he observed near our frequency ω_1 to be the two soft A_1 modes. Taken alone the most natural interpretation of our results (Figs. 7 and 8) is to as-

sociate the two soft A_1 modes with the frequencies ω_1 and ω_2 of Fig. 7. However, still other possibilities exist. For example, both soft A_1 modes could be overdamped in FE and thus lie with the central component of Fig. 7.

III. DETERMINATION OF EIGENVECTORS OF SOFT MODES

It is convenient to discuss the amplitude of the displacements $\vec{u}(\vec{q}lk)$ of the kth atom in the lth unit cell due to a normal vibration of wave vector $\vec{q}$ in terms of the eigenvectors $\vec{E}(\vec{q}k)$ of the dynamical matrix

$$\vec{u}(\vec{q}lk) \propto \vec{E}(\vec{q}k)\, e^{i\vec{q}\cdot\vec{x}(l)}, \tag{4}$$

where $\vec{x}(l)$ is a translation vector of the lattice. In TMO there are two formula units (34 atoms) per unit cell in the PE phase leading to 102 branches in the phonon spectrum. The problem can be further simplified by considering the MoO_4 groups as rigid, reducing the number of degrees of freedom from 102 to 48. It is still necessary to reduce the complexity as much as possible by symmetry considerations. We therefore carried out a group-theoretical study of the normal modes using the multiplier-representation formalism of Maradudin and Vosko.[19] This problem has also been studied recently by Dvorak[30] and Petzelt and Dvorak.[26]

The irreducible multiplier matrix representations of the group of the wave vector $\vec{q}_M = (\frac{1}{2}, \frac{1}{2}, 0)$ (hereafter referred to as the group of M) for PE are shown in Table II.[31] The complex representations $\hat{\tau}_1 = \hat{\tau}_3^*$ and $\hat{\tau}_2 = \hat{\tau}_4^*$ are degenerate by time reversal and may be replaced by real representations $\hat{T}_1$ and $\hat{T}_2$, obtained by a complex unitary transformation. There are thus only three possible physical representations at M, $\hat{T}_1$, $\hat{T}_2$, and $\hat{\tau}_5$, all doubly degenerate. The 48-dimensional vectors $\vec{\psi}$ composed of Cartesian translations and rotations of the contents of a unit cell form the basis for a reducible representation of the group of M. Generating such a representation and using projection operators to decompose this representation into irreducible representations, one can establish that the normal modes at M are distributed into symmetry types as follows: $14\hat{T}_1$, $12\hat{T}_2$, and $22\hat{\tau}_5$.

While it is not essential to do so, it is most convenient to discuss the reduction in symmetry in passing into FE terms of the actual physical displacements $\vec{u}$ given by Eq. (4). The $\vec{u}$ transform like ordinary (as opposed to multiplier) representations[32] T_1, T_2, and τ_5, listed in Table II. Of the symmetry operations listed in Table II, only E and (σ_d, τ) remain in FE. Thus only the displacements $\vec{u}$ which transform like T_2 (or equivalently the eigenvectors $\vec{E}$ of the soft mode which transform like $\hat{T}_2$) can cause the observed symmetry breaking upon condensation. The reduction of $\vec{\psi}$ to basis vectors of T_2 shows that a pair of eigenvectors $(\vec{E}_1, \vec{E}_2)$ is in general composed of six pairs of symmetry-adapted basis functions $(\vec{e}_1^{\,i}, \vec{e}_2^{\,i})$:

$$\vec{E}_1 = \sum_{i=1}^{6} a^i (\vec{e}_1^{\,i} + b^i \vec{e}_2^{\,i}), \quad \vec{E}_2 = \sum_{i=1}^{6} a^i (-b^i \vec{e}_1^{\,i} + \vec{e}_2^{\,i}) . \tag{5}$$

For our choice of basis vectors see Fig. 10. The pairs of eigenvectors given by Petzelt and Dvorak[26] are one set of linear combinations of our $\vec{e}_1^{\,i}$ and $\vec{e}_2^{\,i}$.

The matrix representation of $\hat{T}_2$ which specifies how $\vec{E}_1$ and $\vec{E}_2$ transform among themselves is invariant against an arbitrary real unitary transformation. We will use this feature in Sec. IV, when we discuss an expression for the free energy. The 12 parameters a^i, b^i are not determined by symmetry considerations alone but can be determined by inelastic neutron scattering (dynamical-structure analysis).[33] The eigenvectors $\vec{E}$ are related to the displacements $\vec{u}$ by Eq. (4). The displacements $\vec{u}$ in turn contribute to the inelastic structure factor $F_{\text{inel}}(\vec{Q})$ by

$$F_{\text{inel},i}(\vec{Q}) = \sum_{k}^{\text{unit cell}} b_k(\vec{Q})[\vec{Q}\cdot\vec{u}_i(\vec{q}k)]e^{i\vec{Q}\cdot R_k} . \tag{6}$$

F_{inel} is related to the observed intensity through

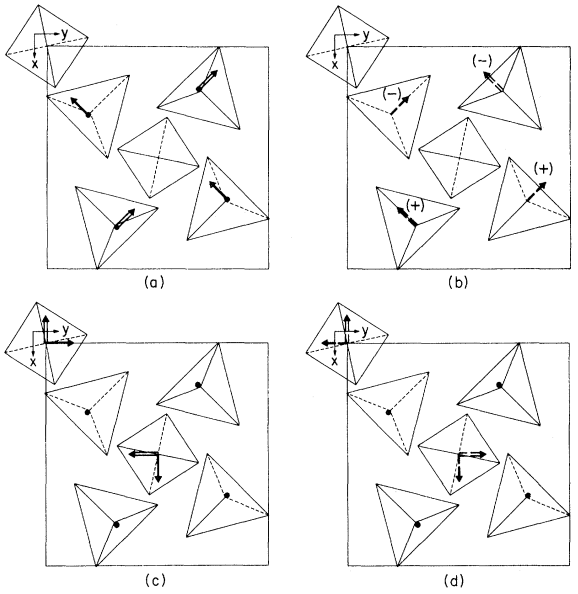

FIG. 10. Basis vectors of the multiplier representation $\hat{T}_2$. A general phonon eigenvector $\vec{E}$ of this symmetry is composed of linear combinations of these vectors. The double-lined arrows represent $\vec{e}_1^{\,i}$, the solid arrows $\vec{e}_2^{\,i}$. Broken arrows indicate rotations. The vector $\vec{E}$ can be grouped into six pairs as follows: (a) $(\vec{e}_1^{\,1}, \vec{e}_2^{\,1})$ translation of the Tb atoms and $(\vec{e}_1^{\,2}, \vec{e}_2^{\,2})$ translation of the general MoO_4 molecules; (b) $(\vec{e}_1^{\,3}, \vec{e}_2^{\,3})$ rotation of the general MoO_4 around an axis in the x-y plane (arrows) and $\vec{e}_1^{\,4}$, $\vec{e}_2^{\,4}$) rotations about z (+ and −); (c) $(\vec{e}_1^{\,5}, \vec{e}_2^{\,5})$ translation of the special MoO_4 molecules; (d) $(\vec{e}_1^{\,6}, \vec{e}_2^{\,6})$ rotation of the special MoO_4.

TABLE II. Multiplier and ordinary representations of the group at the M point $(\frac{1}{2}, \frac{1}{2}, 0)$. The translation $\vec{t}$ is $(\frac{1}{2}, \frac{1}{2}, 0)$. The $\hat{T}_i$ and T_i are physical representations, i.e., reducible into complex irreducible representations.

	E	S_4	C_2	S_4^3	$\sigma_d, \vec{t}$	$\sigma_d', \vec{t}$	$C_{2x}, \vec{t}$	$C_{2y}, \vec{t}$
Multiplier[a]								
$\hat{\tau}_1$	1	$-i$	-1	i	1	-1	i	$-i$
$\hat{\tau}_2$	1	$-i$	-1	i	-1	1	$-i$	i
$\hat{\tau}_3$	1	i	-1	$-i$	1	-1	$-i$	i
$\hat{\tau}_4$	1	i	-1	$-i$	-1	1	i	$-i$
$\hat{\tau}_5$	1 0 0 1	1 0 0 −1	1 0 0 1	1 0 0 −1	0 1 1 0	0 1 1 0	0 −1 1 0	0 −1 1 0
$\hat{T}_1$	1 0 0 1	0 −1 1 0	−1 0 0 −1	0 1 −1 0	1 0 0 1	−1 0 0 −1	0 1 −1 0	0 −1 1 0
$\hat{T}_2$	1 0 0 1	0 −1 1 0	−1 0 0 −1	0 1 −1 0	−1 0 0 −1	1 0 0 1	0 −1 1 0	0 1 −1 0
Ordinary[b]								
T_1	1 0 0 1	0 −1 1 0	−1 0 0 −1	0 1 −1 0	−1 0 0 −1	1 0 0 1	0 −1 1 0	0 1 −1 0
T_2	1 0 0 1	0 −1 1 0	−1 0 0 −1	0 1 −1 0	1 0 0 1	−1 0 0 −1	0 1 −1 0	0 −1 1 0
T_5	1 0 0 1	1 0 0 −1	1 0 0 1	1 0 0 −1	0 −1 −1 0	0 −1 −1 0	0 1 −1 0	0 1 −1 0

[a]Reference 31.

[b]Reference 32.

Eqs. (1) and (2). The integrated intensity I_{int} from the measured intensities of a constant Q scan after appropriate correction for resolution effects[23] (in three-axis measurements) is

$$I_{\text{int}}(\vec{Q}_0) = \int I_{\text{corr}}(\vec{Q}_0, \omega_0)\, d\omega_0 = \int S(Q_0, \omega)\, d\omega$$

$$= \frac{k_B T}{\omega_M^2} \sum_i^2 |F_{\text{inel},i}(\vec{Q}_0)|^2. \qquad (7)$$

In the above expressions $b_k(\vec{Q})$ is the product of the scattering length times a Debye-Waller factor, $\vec{u}_i(qk)$ is the displacement of atom k in mode i with wave vector $\vec{q}$, $\vec{R}_k$ is the equilibrium position of atom k, and ω_M is the frequency of the soft mode.

As the summation in Eq. (6) runs only over one unit cell, we can express $\vec{u}_i$ by $\vec{E}_i$ from Eq. (4). By measuring the intensity of a large number of phonon "reflections" we can determine a best-fitting set of displacement vectors $\vec{u}(\vec{q}, k)$ associated with the soft mode. At a temperature (164 °C) slightly above T_C, the energy transfer is sufficiently small that reliable integrated intensity measurements can be performed on a two-axis spectrometer with a 57-meV incident neutron energy. (We confirmed this fact by repeating several measurements by three-axis spectrometry.) Altogether 68 "reflections" of the type $(h+\frac{1}{2}, k+\frac{1}{2}, 0)$ were studied (see Fig. 11). Of these, the six of type $(h+\frac{1}{2}, h+\frac{1}{2}, 0)$ should vanish for a mode of $\hat{T}_2$ symmetry. The small residual intensity observed at these points is ascribed to multiple scattering due

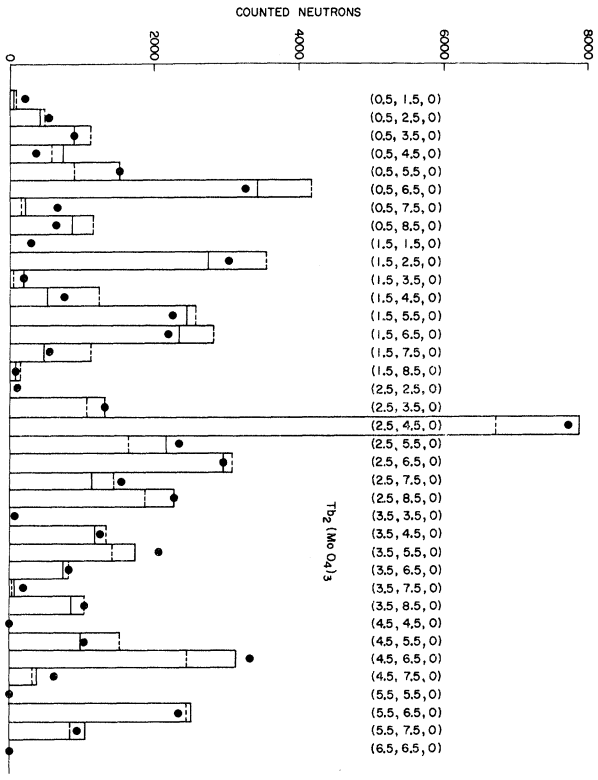

FIG. 11. Phonon "reflections" of the doubly degenerate soft mode in PE at 164 °C (5 °C above T_0). The dashed bars (22% R factor) were calculated with soft-mode eigenvectors derived from static displacements in FE. The solid bars (9.2% R factor) are the results for a best-fitting mode of $\hat{T}_2$ symmetry. (See Table III for the resulting parameters.)

TABLE III. Differences of atomic positions FE − PE from structure determination (Ref. 15) (structure) and the best fit of a condensed soft mode $\vec{E}_1$ to these differences. Atom designation (see Fig. 2) is taken from Jeitschko (Ref. 15).

	Structure	Condensed-mode fit	Structure	Condensed-mode fit	Structure	Condensed-mode fit
PE coord.	x/a	x/a	y/a	y/a	z/c	z/c
Tb atoms						
Tb(1)	0.00496(8)	0.0046	−0.00432(8)	−0.0046	−0.00050(12)	0
Tb(2)	−0.00680(8)	−0.0070	−0.00724(8)	−0.0070	0.00017(12)	0
General MoO_4						
Mo(1)	0.01108(10)	0.0129	−0.01196(10)	−0.0129	−0.00071(10)	0
O(1)	0.0077(12)	0.0078	−0.0149(12)	−0.0078	−0.0016(12)	0
O(3′)	−0.0067(9)	−0.0080	0.0071(9)	0.0080	−0.0003(9)	0
O(6)	0.0450(10)	0.0449	−0.0052(10)	−0.0062	0.0073(10)	0.0041
O(8′)	0.0008(10)	0.0062	−0.0448(10)	−0.0449	−0.0060(10)	−0.0041
Mo(2)	0.00303(10)	0.0043	0.00275(10)	0.0043	−0.00108(10)	0
O(2)	−0.0204(12)	−0.0195	−0.0194(12)	−0.0195	0.0014(12)	0
O(4)	−0.0051(10)	−0.0091	−0.0069(10)	−0.0091	0.0002(10)	0
O(5′)	0.0375(10)	0.0392	0.0005(10)	0.0040	−0.0196(10)	−0.0193
O(7)	0.0020(10)	0.0040	0.0438(10)	0.0392	0.0180(10)	0.0193
Special MoO_4						
Mo(3)	−0.00055(6)	−0.0006	−0.01485(6)	−0.0147	−0.0006(6)	0
O(9)	−0.0060(10)	−0.0054	−0.0184(10)	−0.0154	−0.0024(10)	−0.0015
O(10)	0.0057(10)	0.0023	−0.0169(10)	−0.0138	0.0023(10)	0.0026
O(11)	−0.0045(10)	−0.0054	−0.0111(10)	−0.0154	0.0023(10)	0.0015
O(12)	−0.0014(10)	+0.0023	−0.0118(10)	−0.0138	−0.0027(10)	−0.0026

to higher-order contamination in the beam and was negligible with a (311) Ge monochromator. The remaining 62 intensities were summed pairwise, $I(h,k,0)+I(k,h,0)$. The agreement within pairs was about 5%. Thus we have finally 31 independent intensities, which were used to fit the 12 parameters of the soft mode. This ratio of independent intensities to free parameters is not large. Therefore, we used an initial estimate for these parameters from the static displacements $\vec{U}$ associated with the phase transformation [compare Eq. (4)],

$$\vec{U}(\vec{q}lk) = \eta[\gamma_1\vec{E}_1(\vec{q}k) + \gamma_2\vec{E}_2(\vec{q}k)]e^{i\vec{q}\cdot\vec{x}(l)}, \tag{8}$$

where η is the order parameter and the γ_i describe the linear combination of the two soft modes (degenerate in PE) with eigenvectors $\vec{E}_1$ and $\vec{E}_2$, with $\gamma_1^2+\gamma_2^2=1$.

As we shall show in the discussion of the free energy at a given temperature, we can always choose $\gamma_1=1$, $\gamma_2=0$, i.e.,

$$\vec{U} \propto \vec{E}_1. \tag{9}$$

Therefore we tried to describe the static displacements by a single eigenvector $\vec{E}_1(\hat{T}_2)$ of the most general form (see Fig. 10) with the help of a least-squares fit. Table III gives the static displacements together with the best fit of an $\vec{E}_1(\hat{T}_2)$ mode.

Inspection of Table III reveals that the eigenvector $\vec{E}_1$ cannot fully describe the pattern of static displacements for reasons to be discussed shortly, although it is by far the largest component. The parameters a^i and b^i from Eq. (5) are given in Table IV. We used these 12 values as an initial guess to fit the 31 inelastic integrated intensities. Initially, the displacements were fixed at these values and the phonon reflections fitted by adjusting only a scale factor and two spherical Debye-Waller factors (one for the oxygens, one for the remaining atoms). The result of this fit is shown in Fig. 11 as dashed bars. The agreement is already quite reasonable (22% R factor). If we then adjust the 12 displacement parameters (due to correlation effects not all 12 could be varied simultaneously) the R factor is further reduced to 9.2%. The resulting set of values is given in Table IV. The solid bars in Fig. 11 indicate this best fit.

Tables III and IV show that the static and dynamic displacements are in close correspondence. Some discrepancies are, however, out of the range of the errors, perhaps partially due to the breakdown of the rigid MoO_4 approximation. Another factor which must be borne in mind is that the condensing soft mode couples to other A_1 modes in FE to produce the spontaneous strain and spontaneous polarization. The z displacements of the Tb and MoO_4 ions are certainly due to such coupling to other A_1 modes. Thus there is no rigorous equality between the soft mode and the condensed order parameter in this system.

TABLE IV. Parameters of the soft mode as given by Eq. (5).

		Static	Dynamic
Tb atoms transl.	a^1	-0.0046 ± 0.0006	-0.0047 ± 0.002
	b^1	-1.51 ± 0.05	-1.24 ± 0.8
General MoO_4 transl.	a^2	-0.0129 ± 0.0013	-0.0118 ± 0.001
	b^2	0.34 ± 0.07	0.12 ± 0.2
Rot. in x-y	a^3	0.03 ± 0.01	0.022 ± 0.006
	b^3	4.68 ± 0.2	3.90 ± 1.2
Rot. z	a^4	-0.128 ± 0.007	-0.135 ± 0.005
	b^4	0.86 ± 0.05	0.90 ± 0.06
Special MoO_4 transl.	a^5	0.0147 ± 0.0014	0.020 ± 0.002
	b^5	-0.04 ± 0.08	0.14 ± 0.1
Rot.	a^6	-0.016 ± 0.006	-0.007 ± 0.009
	b^6	-0.21 ± 0.25	-3.34 ± 2.3

IV. FREE-ENERGY CONSIDERATIONS AND $\eta(T)$

The aim of this section is basically to show that the static displacements in FE determined at one given temperature can be described by one eigenvector of the two soft modes condensed out, and to derive an expression describing the temperature dependence of the order parameter η. We use a Landau-Lifshitz approach[34] and to describe a first-order phase transformation we have to include the sixth-order term in the expansion of the free energy F as shown by Devonshire.[35] We restrict ourselves to terms which are necessary to understand the principal features of the phase transformation in $Tb_2(MoO_4)_3$, namely, the shear strain u_{xy} and the spontaneous polarization P_z as well as the primary zone-boundary-phonon displacements:

$$F = \tfrac{1}{2}\omega_M^2\eta^2 + \tfrac{1}{4}\eta^4\textstyle\sum_\alpha V_\alpha f_\alpha^{(4)}(\gamma_i) + \tfrac{1}{6}\eta^6\sum_\alpha W_\alpha f_\alpha^{(6)}(\gamma_i) + \cdots + \tfrac{1}{2}C_{66}^P u_{xy}^2 + \tfrac{1}{2}X_{33}^{-1}P_z^2 + \cdots + \tfrac{1}{2}u_{xy}\eta^2\textstyle\sum_\alpha g_{66,\alpha} f_\alpha^{(2)}(\gamma_i) + a_{36}P_z u_{xy} + \cdots . \quad (10)$$

Here C_{66}^P is the elastic constant at constant polarization, X_{33} the dielectric susceptibility, a_{36} the piezoelectric constant, and ω_M the frequency of the soft mode at the M point. This is the free energy relative to undistorted PE and is written in terms of PE coordinates. $f^{(n)}(\gamma_i)$ represents a function of the two γ_i of order n. Only functions $f^{(4)}(\gamma_i)$, $f^{(6)}(\gamma_i)$, and $u_{xy}f^{(2)}(\gamma_i)$, which transform into themselves under all symmetry operations of PE, are permitted. Explicitly, the functions can be defined as

$$\textstyle\sum_\alpha V_\alpha f_\alpha^{(4)}(\gamma_i) = V_1(\gamma_1^4+\gamma_2^4) + 2V_2\gamma_1^2\gamma_2^2 + 4V_3(\gamma_1^2-\gamma_2^2)\gamma_1\gamma_2 , \quad (11a)$$

$$\textstyle\sum_\alpha W_\alpha f_\alpha^{(6)}(\gamma_i) = W_1(\gamma_1^6+\gamma_2^6) + 3W_2(\gamma_1^2+\gamma_2^2)\gamma_1^2\gamma_2^2 + 6W_3(\gamma_1^2+\gamma_2^2)(\gamma_1^2-\gamma_2^2)\gamma_1\gamma_2 = W_1(\gamma_1^6+\gamma_2^6) + 3W_2\gamma_1^2\gamma_2^2 + 6W_3(\gamma_1^2-\gamma_2^2)\gamma_1\gamma_2 , \quad (11b)$$

$$\textstyle\sum_\alpha g_{66,\alpha} f_\alpha^{(2)}(\gamma_i) = 2g_{66,1}\gamma_1\gamma_2 + g_{66,2}(\gamma_1^2-\gamma_2^2). \quad (11c)$$

With the help of the equilibrium conditions

$$\frac{\partial F}{\partial P_z} = 0$$

and

$$\frac{\partial F}{\partial u_{xy}} = 0 , \quad (12)$$

we find

$$P_z = -a_{36}X_{33}u_{xy}$$

and

$$u_{xy} = -\frac{1}{C_{66}^E}\frac{\eta^2}{2}\sum_\alpha g_{66,\alpha} f_\alpha^{(2)}(\gamma_i) . \quad (13)$$

Here $C_{66}^E = C_{66}^P - a_{36}^2 x_{33}$. We see that P_z is proportional to the strain and the strain in turn proportional to η^2, if we neglect possible variations in the $f_\alpha^{(2)}(\gamma_i)$ discussed later [see Eq. (16)]. Thus the experimental features—that the polarization changes when the strain is switched[5,7] and that the clamped crystal does not show a dielectric anomaly,[4]—are correctly described. The two possible configurations in FE in our notation are expressed by $\pm u_{xy}$.

With the help of Eq. (13), we eliminate P_z and u_{xy} from Eq. (10). We find

$$F = \tfrac{1}{2}\omega_M^2\eta^2 + \tfrac{1}{4}\eta^4\textstyle\sum_\alpha B_\alpha f_\alpha^{(4)}(\gamma_i) + \tfrac{1}{6}\eta^6\sum_\alpha W_\alpha f_\alpha^{(6)}(\gamma_i) + \cdots , \quad (14)$$

where the $f^{(4)}$ have the same form as in Eq. (11a), only the V_α are replaced by the following B_α, where

$$B_1 = V_1 - \frac{g_{66,2}^2}{2C_{66}^E} ,$$

$$B_2 = V_2 - \frac{2g_{66,1}^2 - g_{66,2}^2}{2C_{66}^E} , \quad (15)$$

$$B_3 = V_3 - \frac{g_{66,1}g_{66,2}}{2C_{66}^E} .$$

Making the substitution

$$\gamma_1 = \cos\phi, \quad \gamma_2 = \sin\phi,$$

we minimize F with respect to ϕ, obtaining

$$\tan 4\phi = 4\left(\frac{B_3 + W_3\eta^2}{(B_1 - B_2) + (W_1 - W_2)\eta^2}\right) . \quad (16)$$

We may think of the polar coordinate ϕ as a second order parameter[36] (along with η) for the low-temperature phase. From Eq. (16) it is clear that, in general, ϕ is temperature dependent through $\eta(T)$.

It is possible, although tedious, to carry out a

joint minimization of $F(\eta, \phi)$ for this general case in the basis system $\vec{E}_1$, $\vec{E}_2$ (or γ_1, γ_2). However, as was noted earlier, the degenerate eigenvectors are undefined to within a rotation in the $(\vec{E}_1, \vec{E}_2)$ plane. Thus, if at one temperature we rotate the system by ϕ to $\vec{E}_1'$ and $\vec{E}_2'$ (γ_1', γ_2') we get new B_α' and W_α', such that $B_3' + \eta^2 W_3' = 0$. That leads to the solution $\gamma_1'^2 = 1$, $\gamma_2'^2 = 0$, i.e., $U \propto E_1'$ as used in Eq. (9). In our opinion the statement that $\gamma_i = 0$ solutions are not permissible (Dvorak[37]) is not physically significant given the possibility of such a coordinate transformation.

The solution $\gamma_1'^2 = 1$, $\gamma_2'^2 = 0$ leads to one pair of P_z and u_{xy}, while $\gamma_1'^2 = 0$, $\gamma_2'^2 = 1$ produces the opposite signs of P_z and u_{xy}; $\gamma_1' = \pm 1$ describes two equivalent structures which are microscopically different, as the origins of the unit cells are shifted by $(\frac{1}{2}, \frac{1}{2}, 0)$ in FE coordinates (compare Jeitschko[15]).

A careful search for temperature-dependent changes in ϕ requires precision structural determinations at several temperatures. This is clearly outside the scope of this work. We have therefore chosen to neglect the temperature dependence of ϕ. This is formally accomplished in Eq. (16) by setting either (a) $B_1 - B_2 = B_3 = 0$, (b) $W_1 - W_2 = W_3 = 0$, or (c) $B_3/(B_1 - B_2) = W_3/(W_1 - W_2)$. [The first two conditions represent isotropy of the fourth- or sixth-order terms, respectively, whereas (c) equates the degree of anisotropy of the fourth- and sixth-order terms.] It is not necessary for our purposes to speculate or choose among (a)–(c) at this time. For illustrative purposes at a later stage we will make assumption (b). We justify our treatment on the following pragmatic considerations: (i) The fact that several superlattice intensities were observed to have nearly identical relative temperature dependences suggests that $\phi \approx$ const. (ii) As we will proceed to show, the behavior of $\eta(T)$ determined experimentally is in reasonable agreement with the assumption that ϕ is temperature independent.

We now assume $\phi = \text{const} = 0$ [Eq. (16)]. That is to say, the coordinate system is already chosen such that $\gamma_1 = 1$, $\gamma_2 = 0$, and the resulting displacements are given entirely in terms of the component $\vec{E}_1$. In this coordinate system the free energy assumes the simple familiar form

$$F = \tfrac{1}{2}\chi\eta^2 + \tfrac{1}{4}\xi\eta^4 + \tfrac{1}{6}\zeta\eta^6 + \cdots , \tag{17}$$

where $\chi = \omega_M^2$, $\xi = B_1$, and $\psi = W_1$. As is well known, for first-order transformations the parameters must satisfy the conditions $\xi < 0$, $\zeta > 0$. At the transition temperature the values of the order parameter η_0 and reciprocal susceptibility χ_0 in FE are

$$\eta_0^2 = \tfrac{3}{4}(-\xi/\zeta), \quad \chi_0 = \tfrac{3}{16}\xi^2/\zeta \ . \tag{18}$$

With the help of Eq. (18) we can write for any temperature less than the transformation temperature T_0

$$\eta^2 = \tfrac{2}{3}\eta_0^2 + \left(\tfrac{4}{9}\eta_0^4 - \tfrac{1}{3}\eta_0^4\frac{\chi}{\chi_0}\right)^{1/2} . \tag{19}$$

The assumed temperature dependence of χ leads to

$$\frac{\chi}{\chi_0} = \frac{T - T_C}{T_0 - T_C} \ . \tag{20}$$

For $T \leq T_0$ we find

$$\eta^2 = \tfrac{1}{3}\eta_0^2\left[2 + \left(4 - 3\,\frac{T - T_C}{T_0 - T_C}\right)^{1/2}\right] . \tag{21}$$

If the static displacements are small $(\vec{Q}\cdot\vec{U} < 1)$, the intensity of a superlattice reflection is proportional to η^2. Thus a comparison of the temperature dependence of the superlattice intensities with $\eta(T)$ predicted from Eq. (21) characterizes the behavior of the order parameter in terms of the familiar Landau free energy. A small cylindrical sample (0.15-cm diam, 0.8-cm length) was used to eliminate extinction corrections. Submultiple beam contamination, although minimized by a pyrolytic-graphite filter,[24] was not entirely negligible because of the weakness of the superlattice reflections. Appropriate corrections (varying from 1 to 16%) were deduced both from a study of spurious intensity at forbidden superlattice positions and from residual Bragg intensity which persisted into the PE phase at the superlattice positions. Below T_0 the sample is composed of unknown fractions of opposite FE domains, and these fractions may change with temperature. However, since opposite domains exchange a and b axes, the sum $I(hkl) + I(khl)$ is independent of the domain distribution. We therefore chose two Bragg pairs, (320)+(230) and (520)+(250) (FE indexing), for study vs temperature. A triple-axis spectrometer (set for $\Delta E = 0$) was used to reduce the inelastic (critical-scattering) background. The data were fitted to Eq. (21) by a least-squares procedure. The results, in which (besides an arbitrary scale factor) T_C was adjustable, are shown in Fig. 12. Larger values of T_0 gave distinctly poorer fits. The four values for T_C given in Fig. 12 are close to each other but differ somewhat from the $T_C = (149 \pm 2)\,^\circ\text{C}$ as determined from the Curie-Weiss law in the PE phase. This may be indicative of slight inadequacies in the Landau theory, which does not in principle properly account for fluctuation effects in either the susceptibility (i.e., in ω_M^{-2}) or the order parameter near T_0, but may also indicate the limit of the validity of the assumption that ϕ is temperature independent.

The temperature dependence of the spontaneous polarization and x-y shear as measured by Cummins[5] is also shown in Fig. 12. We may draw two conclusions: (a) Polarization, shear angle, and

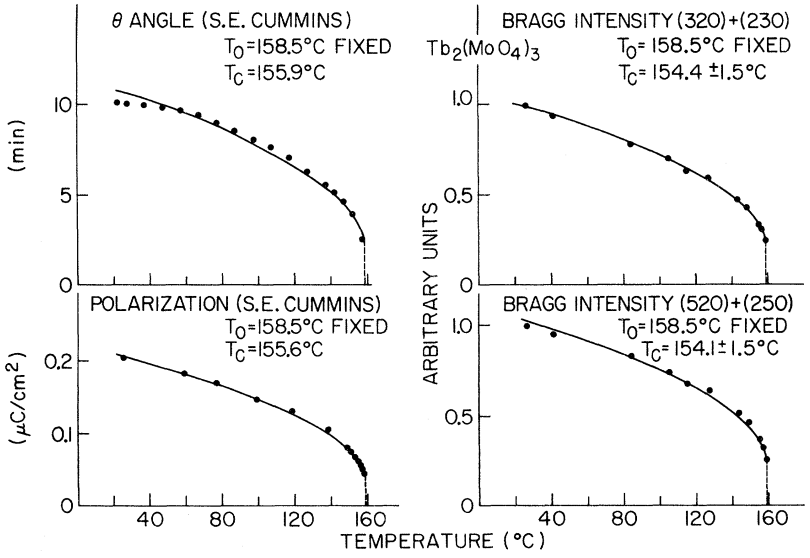

FIG. 12. Temperature dependence of three physical quantities which have been used to characterize the phase transformation in rare-earth molybdates. All have been fitted with Eq. (21). The good resulting fit shows that the spontaneous strain and spontaneous polarization are proportional to the square of the zone-boundary soft-mode displacements.

Bragg intensity have the same temperature dependence; (b) all these quantities can be described by Eq. (21); i.e., they are functions of the order parameter squared. Thus in TMO the magnitude of the antiferroelectric displacements $\vec{U}$, not the polarization itself, is a suitable order parameter in that it displays the temperature dependence predicted by a Landau-like free-energy expression.

V. ELASTIC PROPERTIES

Cross *et al.*[4] reported anomalous temperature dependence of C_{66}^{PE} near T_0 in $Gd_2(MoO_4)_3$ (GMO). (The superscript PE here indicates only that the elastic constants are referred to PE coordinates. C^{PE} is well defined in both PE and FE phases.) A similar effect occurs in C_{11}^{FE} since the two quantities are symmetry related.[5,20] It is therefore of interest to compare the ultrasonic elastic behavior with much-higher-frequency "hypersonic" behavior derived from the initial velocities of the acoustic phonons as determined by neutron scattering. Five of the six existing constants in PE could be derived from the squares of measured velocities as shown in Table V. C_{13}^{PE} was obtained indirectly from the velocity of a $\vec{q}=[\xi\xi\xi]$ branch of undetermined polarization, by insisting that it satisfies the Christoffel equation[38] for the [111] direction. This led to two possible values of C_{13}^{PE}, of which only one satisfies the necessary stability conditions.[39] The PE elastic constants are given in Table VI.

The diagonal elastic constants C_{11}^{FE} have been measured at room temperature in GMO by Epstein *et al.*[20] Making due allowance for the temperature dependence of C_{11}^{FE} (see below), our data for TMO are in quite close agreement, except for C_{66}^{FE}, for which our values are some 20% higher in both PE and FE. We have no explanation for the discrepancy. One possible source of systematic discrepancy we looked into is the renormalization of the elastic constant due to piezoelectric coupling. The effective elastic constants depend explicitly upon the direction of plane-wave propagation in this case.[38] For example, in tetragonal TMO the velocity of modes polarized along [110] and propagating along [001] is determined by C_{44}^{PE}. For modes with polarization and propagation vectors reversed the effective elastic constant is $C_{44}^{PE}+4\pi B_{14}^2/\epsilon_1$, where B_{14} and ϵ_1 are elements of the piezoelastic and dielectric tensors, respectively. While such differences can be quite important in some ferroelectrics,[40] we find no observable difference in TMO for C_{44}^{PE} measured in these two ways. Cummins[5] also found no detectable piezoelectric effects on the elastic constants he studied in GMO.

We studied the temperature dependence of $C_{66}^{PE}=A$ (Table V) at temperatures between 20 and 130 °C and found no change within our accuracy. Furthermore, the values in PE and FE we find to be comparable. We take this as an indication that the anomalous temperature dependence seen clearly at lower frequencies (although, to be sure, as yet only in GMO) is less pronounced at hypersonic frequencies. However, a really definitive neutron study of this behavior very near T_0 was not attempted.

VI. CONCLUDING REMARKS

Using neutron-diffraction techniques, we have been able to test and confirm in a direct and unambiguous way the recently suggested mechanism for ferroelectric phase transformations in rare-earth molybdates. It is now clear that these materials furnish nice examples of displacive phase

TABLE V. Elastic properties of $Tb_2(MoO_4)_3$ in the paraelectric (PE) and the ferroelectric (FE) phase (transition temperature $T_0 = 159\,°C$).

Temperature (°C)	Direction[a] of $\vec{q}$	Direction[a] of polarization	Velocity v (10^5 cm sec^{-1})	ρv^2[b] (10^{11} dyn cm^{-2})	Equality of ρv^2 in PE	Equality of ρv^2 in FE
260	[110]	[1$\bar{1}$0]	2.60	3.11 ± 0.15	$\frac{1}{2}(C_{11}^{PE} - C_{12}^{PE})$	C_{66}^{FE}
260	[110]	[110]	4.39	8.9 ± 0.45	$\frac{1}{2}(C_{11}^{PE} + C_{12}^{PE} + 2C_{66}^{PE})$	$C_{11,22}^{FE}$
184 295	[001]	[001]	4.68	10.1 ± 0.9	C_{33}^{PE}	C_{33}^{FE}
184	[110]	[001]	2.37	2.60 ± 0.13	C_{44}^{PE}	$C_{44,55}^{FE}$
295	[110]	[001]	2.39	2.64 ± 0.13	C_{44}^{PE}	$C_{44,55}^{FE}$
184	[001]	[110]	2.40	2.67 ± 0.13	C_{44}^{PE}	$C_{44,55}^{FE}$
260	[100]	[010]	2.49	2.87 ± 0.15	C_{66}^{PE}	A[c]
184	[111]	in (*hhl*) plane	1.80	1.49 ± 0.15		B[c]
20	[100]	[010]	2.61	3.15 ± 0.2	$\frac{1}{2}(C_{11}^{PE} - C_{12}^{PE})$	C_{66}^{FE}
20	[100]	[001]	2.37	2.60 ± 0.15	C_{44}^{PE}	$C_{44,55}^{FE}$
20	[1$\bar{1}$0]	[110]	2.45	2.77 ± 0.25	C_{66}^{PE}	A[c]

[a] Coordinate system in PE is rotated by 45° with respect to that of FE.

[b] We used density $\rho = 4.62$ g cm^{-3}, Ref. 3.

[c] $A = \frac{1}{4}(C_{11}^{FE} + C_{22}^{FE} + 2C_{66}^{FE}) - \frac{1}{4}[(C_{11}^{FE} - C_{22}^{FE})^2 + 4(C_{12}^{FE} + C_{66}^{FE})^2]^{1/2}$,

$B = \frac{1}{4}(C_{11,22}^{FE} + C_{33}^{FE} + 2C_{44,55}^{FE}) - \frac{1}{4}[(C_{11,22}^{FE} - C_{33}^{FE})^2 + 4(C_{13,23}^{FE} + C_{44,55}^{FE})^2]^{1/2}$.

transformations. There are, however, some novel features which distinguish them from other displacive transformations which have been studied previously. Unlike the perovskite ferroelectrics, for example, in these materials the primary order parameter (by which we mean the parameter associated with the soft mode, and which therefore shows large fluctuations near T_C) has no macroscopic polarization, but is instead antipolar and seemingly unrelated to the ferroelectric phase which is produced.

Antipolar displacements resulting from a short-wavelength phonon instability are not new. What is different is the particular combination of induced secondary (perhaps we should say secondary and tertiary) order parameters which constitute the spontaneous strain and polarization. If there is a general lesson to be learned, it is the importance of distinguishing between primary and secondary order parameters, and second the richness of behavior which the secondary parameters make possible. As Cochran[41] has recently emphasized, the possibility of secondary order parameters is an elaboration not contained in Landau's original discussion of phase transformations.

The rare-earth molybdates also differ from the other well-studied materials undergoing displacive phase changes in that the composition of the spontaneous displacements, expressed in terms of the degenerate soft-mode eigenvectors, is not fixed by symmetry considerations but is governed by a pair of coupled equations. This allows for a continuous variation in both the magnitude of the order parameter (η) and its direction (ϕ) in the space of a fixed set of eigenvectors ($\vec{E}_1$, $\vec{E}_2$). ϕ may be called a secondary order parameter as well as those discussed in the foregoing paragraph. We have shown that the temperature dependence of η is described reasonably well by an approximation which renders ϕ temperature independent, but we know of no fundamental reason why this is so. Undoubtedly, therefore, other materials exist or will be found in which this interesting complication of a varying angle ϕ coupled with the order parameter cannot be so easily dealt with.

ACKNOWLEDGMENTS

We would like to thank Dr. L. Brixner for lending us the TMO crystal and Dr. W. Jeitschko for a preprint of unpublished work. It is a pleasure to acknowledge stimulating discussions with Professor W. Cochran and illuminating discussions with Dr. J. Sivardière and Dr. A. Hüller.

APPENDIX

We wish to work out the soft-mode frequencies associated with the free energy given in Eq. (14), which, written explicitly, is

$$F = \tfrac{1}{2}\omega_M^2\eta^2(\gamma_1^2 + \gamma_2^2) + \tfrac{1}{4}B_1\eta^4(\gamma_1^4 + \gamma_2^4) + \tfrac{1}{2}B_2\eta^4\gamma_1^2\gamma_2^2$$

TABLE VI. Elastic constants in the tetragonal phase (PE) at 260 °C in 10^{11} dyn cm^{-2}.

C_{11}	C_{33}	C_{12}	C_{13}	C_{44}	C_{66}
9.1 ± 0.5	10.1 ± 0.9	2.9 ± 0.5	6.7 ± 0.7	2.65 ± 0.10	2.87 ± 0.15

$$+\tfrac{1}{6}W_1\eta^6(\gamma_1^6+\gamma_2^6)+\tfrac{1}{2}W_2\eta^6(\gamma_1^4\gamma_2^2+\gamma_1^2\gamma_2^4)+\cdots. \quad \text{(A1)}$$

As discussed in the text we assume that the parameters are such that the equilibrium conditions $\partial F/\partial(\eta\gamma_1)=\partial F/\partial(\eta\gamma_2)=0$ are satisfied in FE with γ_1/γ_2 independent of temperature. With no further loss of generality, the basis vectors can be chosen such that $\gamma_1=1$, $\gamma_2=0$. The soft-mode frequencies are simply related to the curvature of the free energy about its minimum:

$$\omega_1^2=\left.\frac{\partial^2 F}{\partial(\eta\gamma_1)^2}\right|_{\gamma_1^2=1,\ \gamma_2^2=0},\qquad \omega_2^2=\left.\frac{\partial^2 F}{\partial(\eta\gamma_2)^2}\right|_{\gamma_1^2=1,\ \gamma^2=0}. \quad \text{(A2)}$$

We find

$$\omega_1^2=\omega_M^2(T)+3B_1\eta^2+5W_1\eta^4, \quad \text{(A3a)}$$

$$\omega_2^2=\omega_M^2(T)+B_2\eta^2+W_2\eta^4. \quad \text{(A3b)}$$

These frequencies are degenerate in PE ($\eta=0$), but in general this degeneracy is removed in FE. At the transition temperature T_0 [compare Eq. (18)],

$$\omega_{M0}^2=\omega_M^2(T_0)=\tfrac{3}{16}(B_1^2/W_1), \quad \text{(A4)}$$

$$\eta_0^2=\eta^2(T_0)=-\tfrac{3}{4}(B_1/W_1), \quad \text{(A5)}$$

$$\omega_{10}^2=\omega_1^2(T_0)=4\omega_{M0}^2, \quad \text{(A6)}$$

$$\omega_{20}^2=\omega_2^2(T_0)=\omega_{M0}^2[1+3(W_2/W_1)-4(B_2/B_1)]. \quad \text{(A7)}$$

If we assume that ω_M^2 depends linearly on the temperature in FE as found in PE, we can write Eqs. (20) and (21) for $T\leq T_0$:

$$\omega_M^2=\omega_{M0}^2\,\frac{T-T_C}{T_0-T_C}, \quad \text{(A8)}$$

$$\eta^2=\tfrac{1}{3}\eta_0^2\left[2+\left(4-3\,\frac{T-T_C}{T_0-T_C}\right)^{1/2}\right]. \quad \text{(A9)}$$

The soft-mode frequencies in FE are then given by

$$\omega_1^2=\tfrac{16}{3}\,\omega_{M0}^2\left[1-\tfrac{3}{4}\,\frac{T-T_C}{T_0-T_C}+\left(1-\tfrac{3}{4}\,\frac{T-T_C}{T_0-T_C}\right)^{1/2}\right], \quad \text{(A10)}$$

$$\omega_2^2=\tfrac{16}{3}\,\omega_{M0}^2\left[\frac{1}{2}\left(\frac{W_2}{W_1}-\frac{B_2}{B_1}\right)+\frac{3}{16}\left(1-\frac{W_2}{W_1}\right)\times\frac{T-T_C}{T_0-T_C}+\frac{1}{2}\left(\frac{W_2}{W_1}-\frac{B_2}{B_1}\right)\times\left(1-\frac{3}{4}\,\frac{T-T_C}{T_0-T_C}\right)^{1/2}\right]. \quad \text{(A11)}$$

ω_1 in FE is the frequency of the mode representing fluctuations in the order parameter {eigenvector proportional to the static displacements [Eq. (8)]} and ω_2 is the frequency of the orthogonal mode which has no average static value.

In order to get some impression of the behavior of ω_2 given by (A11) we can make what is perhaps the simplest of the three decoupling assumptions mentioned in Sec. IV; namely, isotropy in the sixth-order terms $W_1=W_2$. The behavior of ω_1 and ω_2 for different ratios of B_2/B_1 is shown in Fig. 9. (The conditions $B_1\leq 0$ and $B_1\leq B_2$ are necessary for the equilibrium solution $\gamma_1^2=1$, $\gamma_2^2=0$.)

†Work performed under the auspices of the U. S. Atomic Energy Commission.

*Guest scientist on leave from Institut für Festkörperforschung, Kernforschungsanlage-Jülich, Germany, now returned.

[1]H. J. Borchardt and P. E. Bierstedt, J. Appl. Phys. 38, 2057 (1967).

[2]We choose $Tb_2(MoO_4)_3$ (TMO) rather than the more extensively studied $Gd_2(MoO_4)_3$ (GMO) because of more favorable neutron-scattering properties. Those two compounds have very similar behavior.

[3]E. T. Keve, S. C. Abrahams, K. Nassau, and A. M. Glass, Solid State Commun. 8, 1517 (1970).

[4]L. E. Cross, A. Fouskova, and S. E. Cummins, Phys. Rev. Letters 21, 812 (1968).

[5]S. E. Cummins, Ferroelectrics 1, 11 (1970).

[6]A. W. Smith and G. Burns, Phys. Letters 28A, 501 (1969).

[7]A. Kumada, H. Yumoto, and S. Ashida, J. Phys. Soc. Japan Suppl. 28, 351 (1970).

[8]K. Aizu, J. Phys. Soc. Japan 27, 387 (1969).

[9]K. Aizu, A. Kumada, H. Yumoto, and S. Ashida, J. Phys. Soc. Japan 27, 511 (1969).

[10]E. Pytte, Solid State Commun. 8, 2101 (1970).

[11]A. P. Levanyuk and D. G. Sannikov, Fiz. Tverd. Tela 12, 2997 (1970) [Sov. Phys. Solid State 12, 2418 (1971)].

[12]K. Aizu, J. Phys. Soc. Japan 31, 802 (1971).

[13]J. D. Axe, B. Dorner, and G. Shirane, Phys. Rev. Letters 26, 519 (1971).

[14]E. T. Keve, S. C. Abrahams, and J. L. Bernstein, J. Chem. Phys. 54, 3185 (1971).

[15]W. Jeitschko, Naturwiss. 27, 544 (1970); Acta Cryst. B28, 60 (1972).

[16]R. E. Newnham, H. A. Mckinstry, C. W. Gregg, and W. R. Still, Phys. Status Solidi 32, K49 (1969).

[17]H. J. Borchardt and P. E. Bierstedt, Appl. Phys. Letters 8, 50 (1966).

[18]K. Nassau, H. J. Levinstein, and G. M. Loiacono, J. Phys. Chem. Solids 26, 1805 (1965).

[19]A. A. Maradudin and S. H. Vosko, Rev. Mod. Phys. 40, 1 (1968).

[20]D. J. Epstein, W. Y. Herrick, and R. F. Turek, Solid State Commun. 8, 1491 (1970).

[21]M. J. Cooper and R. Nathans, Acta Cryst. 23, 357 (1967).
[22]S. M. Shapiro (private communication).
[23]B. Dorner, Acta Cryst. A (to be published).
[24]V. J. Minkiewicz and G. Shirane, Nucl. Instr. Methods 89, 109 (1970).
[25]W. Cochran, Advan. Phys. 18, 157 (1969).
[26]J. Petzelt and V. Dvorak, Phys. Status Solidi 46, 413 (1971).
[27]J. Petzelt, Solid State Commun. 9, 1485 (1971).
[28]P. A. Fleury, Solid State Commun. 8, 601 (1970); I. W. Shepherd, *ibid.* 9, 1857 (1971).
[29]J. M. Worlock (private communication).
[30]V. Dvorak, Phys. Status Solidi 45, 147 (1971).
[31]O. V. Kovalev, *Irreducible Representations of the Space Groups* (Gordon and Breach, New York, 1965).
[32]S. C. Miller and W. F. Love, *Tables of Irreducible Representations of Space Groups and Co-Representations of Magnetic Space Groups* (Pruett, Boulder, Colo., 1967).
[33]J. Harada, J. D. Axe, and G. Shirane, Acta Cryst. A26, 608 (1970).
[34]L. D. Landau and E. M. Lifshitz, *Statistical Physics* (Addison-Wesley, Reading, Mass, 1969).
[35]A. F. Devonshire, Advan. Phys. 3, 85 (1954).
[36]The a^i and b^i are temperature independent as long as there is no coupling of the $\vec{E}_1$ and $\vec{E}_2$ to other modes within the same representation.
[37]V. Dvorak, Phys. Status Solidi 46, 763 (1971).
[38]L. D. Landau and E. M. Lifshitz, *Electrodynamics of Continuous Media* (Pergamon, New York, 1960), p. 79.
[39]M. Born and K. Huang, *Dynamical Theory of Crystal Lattices* (Clarendon, Oxford, 1962).
[40]G. Shirane, J. D. Axe, J. Harada, and A. Linz, Phys. Rev. B 2, 3651 (1970).
[41]W. Cochran, in *Structural Phase Transitions and Soft Modes*, edited by E. J. Samuelsen, E. Andersen, and J. Feder (Universtetsforlaget, Oslo, 1971).

PHYSICAL REVIEW B VOLUME 6, NUMBER 5 1 SEPTEMBER 1972

New Inequalities among the Critical-Point Exponents for the Spin-Spin and Energy-Energy Correlation Functions*†

Luke L. Liu‡ and Richard I. Joseph
Department of Electrical Engineering, The Johns Hopkins University, Baltimore, Maryland 20218

and

H. Eugene Stanley
Physics Department, Massachusetts Institute of Technology, Cambridge, Massachusetts 02139
(Received 5 November 1971; revised manuscript received 27 March 1972)

Two new inequalities, (i) $\gamma' \geq 2\beta(2-\eta)/(d-2+\eta) + 2\phi[2\beta/(d-2+\eta) - \nu'_\phi]$ and (ii) $(\delta-1)/\delta \geq 2(2-\eta)/\delta(d-2+\eta) + 2\phi[2/\delta(d-2+\eta) - \mu_\phi]$, are derived among critical-point exponents that describe the behavior of the two-spin correlation function $C_2(T,H,\vec{r}) \equiv \langle s_0^z s_{\vec{r}}^z\rangle - \langle s_0^z\rangle \langle s_{\vec{r}}^z\rangle$, subject to plausible assumptions (rigorous for Ising magnets). Here ν'_ϕ and μ_ϕ describe the divergence as $T \to T_c^-$ and as $H \to 0^+$, respectively, of the "generalized correlation length" $\xi_\phi(T,H)$, defined as the 2ϕth root of the normalized 2ϕth spatial moment of $C_2(T, H, \vec{r})$. Also derived are the corresponding inequalities among exponents that describe the behavior of the energy-energy correlation function. Inequality (i) is shown to lead to an inequality between primed and unprimed exponents. Moreover, if ν'_ϕ is independent of ϕ, then (i) implies that $\nu' \geq 2\beta/(d-2+\eta)$ and $\gamma' \geq (2-\eta)\nu'$, while if μ_ϕ is independent of ϕ, then (ii) implies $\mu \geq 2/\delta(d-2+\eta)$ and $(\delta-1)/\delta \geq (2-\eta)\mu$.

I. INTRODUCTION

Rigorous inequalities among critical-point exponents[1] have served to assist in the interpretation of experimental data and, perhaps more significant historically, have contributed to the formulation of the static scaling hypothesis[2] (which has the feature that most inequalities are predicted to be satisfied as equalities).

These inequalities may be classified into two groups: (i) relations among critical-point exponents characterizing the behavior of thermodynamic functions,[1] and (ii) relations among exponents characterizing the behavior of the static correlation functions.[3-5]

Inequalities belonging to category (i) (e.g., $\alpha' + 2\beta + \gamma' \geq 2$) are frequently found to be satisfied as *equalities* by experimental results *and* by calculations on model systems.[6] On the other hand, certain of the inequalities belonging to category (ii) are almost invariably *not* obeyed as equalities, with the notable exceptions of the two-dimensional Ising model ($d=2$) and the three-dimensional spherical model. Thus, for example, $d\nu \geq 2-\alpha$ is satisfied as an equality for the $d=2$ Ising model ($\nu=1$, $\alpha=0$), but for the $d=3$ Ising model, numerical-approximation methods indicate that $d\nu$ is about 2% larger than $2-\alpha$.[7]